Structural and Magnetic Properties of Fe_2O_3 Nanoparticles Dispersed over a Silica Matrix

C. Cannas,[†] D. Gatteschi,[‡] A. Musinu,*[,†] G. Piccaluga,[†] and C. Sangregorio[‡]

Dipartimento di Scienze Chimiche, Universitá, Via Ospedale 72, 09124 Cagliari, Italy, and Dipartimento di Chimica, Universita′, Via Maragliano 75, 50144 Firenze, Italy

Received: March 4, 1998; In Final Form: June 12, 1998

The structure and the magnetic properties of a series of $Fe_2O_3-SiO_2$ nanocomposites (9−33 wt % Fe_2O_3), prepared by a sol−gel method and submitted to thermal treatments in the temperature range 300−900 °C, were investigated through XRD, TEM, EPR, and magnetic susceptibility measurements. Superparamagnetic iron(III) oxide nanoparticles with a narrow size distribution, dispersed over the amorphous silica matrix, are present in all the samples. They are mostly amorphous, antiferromagnetic in the samples treated at low temperatures. At $T > 700$ °C, a lot of γ-Fe_2O_3 crystalline ferrimagnetic nanoparticles (4−6 nm) are formed, while a further increase of the temperature results in the γ- to α-Fe_2O_3 transformation. The variation of iron oxide content affects the abundance of γ-Fe_2O_3 formation, which reaches the maximum percent values in the more dilute samples. In the more concentrated samples, while the amount of maghemite is still growing, antiferromagnetic α-Fe_2O_3 begins to form. As a consequence, the saturation magnetization lowers in the samples with higher Fe_2O_3 content. Also, interparticle interactions, evidenced by fitting susceptibility values versus temperature and by EPR observations, contribute to such a decrease.

Introduction

γ-Fe_2O_3 (maghemite) has attracted technological interest due to its magnetic and catalytic properties. Interest has increased following the observation that the properties are strongly dependent on the size of the particles, with dramatic changes when nanometric sizes are reached.[1−6]

The preparation of pure nanophase γ-Fe_2O_3 presents some difficulties partially arising from the different metal oxidation states, which can lead to the contemporary presence of various oxides (FeO, Fe_2O_3, and Fe_3O_4). Moreover, Fe_2O_3, besides the maghemite form, also exhibits amorphous or other crystalline phases, among which hematite (α-Fe_2O_3) is the one that is thermodynamically stable; γ-Fe_2O_3 transforms in the α-Fe_2O_3 phase at temperatures above 380 °C. Finally, γ-Fe_2O_3 nanoparticles tend to aggregate with a consequent increase of the particle size, which makes the γ-to-α transition easier.[7]

Attempts have been made to stabilize nanometric γ-Fe_2O_3 particles by dispersing maghemite in a polymeric, glassy, or ceramic matrix.[8−14] They have had different success, and all of them require rather complicated processing.

In a recent paper,[15] we reported the preparation of an $Fe_2O_3-SiO_2$ composite, containing ∼17 wt % Fe_2O_3, through a very simple sol−gel method, previously proposed for the synthesis of $Me-SiO_2$ systems (Me = metal)[16−18] and also used for the synthesis of $Fe_2O_3-SiO_2$ nanocomposites.[19−21] A multitechnique approach, by XRD, TEM, Mössbauer spectroscopy, EPR, and magnetic susceptibility measurements, was used to characterize the structure and the magnetic properties of the intermediate and final products. Superparamagnetic iron(III) oxide nanoparticles were obtained. They are X-ray amorphous and antiferromagnetic in the samples treated at low temperatures, while they convert to crystalline ferrimagnetic γ-Fe_2O_3 after treatment at $T > 700$ °C. At temperatures higher than 900 °C, α-Fe_2O_3 formation was also observed. The adopted method is certainly able to give rise to particles having the required small size but presents some difficulties in obtaining systems where only the maghemite phase is present. In fact, the whole result suggests a slow and continuous transition from amorphous to γ-Fe_2O_3 to α-Fe_2O_3 in the course of thermal treatments and the presence of more than one oxide phase in the various samples, although maghemite prevails in the composite treated at 900 °C. These facts lead to different experimental evaluations of the transition temperature.

In this paper, the study of a series of samples with different iron oxide contents is reported. The main aim of the work is to verify if the change of composition in a wide range (from 9 to 33 wt % Fe_2O_3) influences the average size of the particles and/or their size distribution. Since the particle size affects the phase transition,[7] an additional purpose is to verify if the abundance of maghemite phase and the magnetic properties of the samples change with composition.

Experimental Section

A series of iron oxide/silica composites were prepared by mixing an alcoholic solution of TEOS (Aldrich, 98%) and aqueous solutions of iron nitrate ($Fe(NO_3)_3 \cdot 9H_2O$, Aldrich, 98%), following the previously described procedure.[15] Different iron oxide contents were obtained by modification of the iron nitrate concentration in the aqueous solution, while the alcohol/TEOS/water molar ratio was gradually modified from 3.85/1/10.6 in the most dilute system up to 3.85/1/13.3 in the most concentrated one.

The pH of the mixtures was 0.9 in each system. The high acidity, necessary to prevent the precipitation of the iron hydroxides, determines a relatively long gelation time (about 9 days) in all the preparations. After 1 h of stirring, the clear sols were poured into a Teflon beaker and allowed to gel in air. The gels were dried in an oven for about 1 week while the temperature was slowly raised to 100 °C. The dried samples

[†] Universitá, Via Ospedale, Cagliari.
[‡] Universitá, Via Maragliano, Firenze.

S1089-5647(98)01355-8 CCC: $15.00
Published on Web 09/17/1998

were then powdered and kept 24 h at 150 °C in order to decompose the nitrate and to eliminate residual water and solvents. The samples were then heated at higher temperatures, with steps of 50 °C up to 500 °C and of 100 °C up to 900 °C, and kept 30 min at each temperature.

Five samples were prepared, containing respectively 9.1, 16.9, 23.0, 28.5, and 33.2 wt % Fe_2O_3. The labels Fe_xY will be used in the following, where Y indicates the treatment temperature (T_{treat}) and x the composition.

The structural evolution of the samples, as a function of T_{treat} and composition, was monitored by XRD using $\theta-2\theta$ conventional equipment (Siemens D500) with a Mo Kα wavelength; iron oxide nanoparticles were observed in electron micrographs obtained by a TEM (JEOL 200CX), operating at 200 kV.

Static magnetic susceptibilities were measured with a Metronique Ingeniérie MS02 SQUID magnetometer equipped with a superconducting magnet capable of producing fields up to 8 T. Zero-field-cooled (ZFC) magnetizations were measured by cooling the sample in zero field and then by increasing the temperature with an applied field of 50 Oe, while field-cooled curves (FC) were collected by cooling the sample in the measuring field of 50 Oe.

The EPR measurements were performed on a Varian E9 spectrometer working at the X-band (9.25 GHz) and equipped with an Oxford cryostat that allowed temperature variations from 4 K to room temperature. The sample powders were dispersed in a paraffin matrix to prevent orientation of the crystallites along the Zeeman magnetic field, as observed in preliminary experiments.

Results

TEM and XRD. TEM observations show the presence of iron oxide nanoparticles dispersed over the silica matrix in all the samples. The amount of visible particles slightly increases with the iron oxide content and with T_{treat}, while their size increases from an average value of about 2 nm up to an average of about 6 nm and the size distribution becomes less narrow. The dark field micrographs also indicate the amorphous character of the greatest part of the nanoparticles in the samples treated at lower temperatures, in contrast with the crystalline character of most particles present in the samples treated at higher temperatures. As an example, bright and dark field micrographs of the $Fe_{28.5}900$ sample are reported in parts a and b of Figure 1, indicating the crystalline character of the nanoparticles homogeneously distributed over the silica support.

The TEM micrograph of the $Fe_{33.2}300$ sample (Figure 2) exhibits groups of parallel rows of oxide nanoparticles which are not present in the other samples. It is likely that the high iron oxide content gives rise to such a number of nanoparticles which do not allow a homogeneous distribution in the host silica matrix.

The XRD spectra of the samples treated at 300 °C are reported in Figure 3. In agreement with the TEM observations, the spectra are typical of amorphous materials. With increasing iron oxide content, however, two broad peaks emerge over the pattern of the amorphous silica. The intensity of these peaks slowly rises with T_{treat} and for the $Fe_{9.1}$, $Fe_{16.9}$, and $Fe_{23.0}$ samples becomes comparable to those of $Fe_{28.5}300$ and $Fe_{33.2}300$ respectively only at 800, 600, and 500 °C. In any case, the signals are very broad, indicating the presence of nanoparticles of iron oxide, at the limits of observation of the XRD analysis (3−4 nm). The position of these bands is consistent with the d spacing typical of most iron hydroxides, oxyhydroxides, or oxides. However, since the result of the magnetic measurements, reported in the following, shows the formation of a ferrimagnetic phase at $T_{treat} > 700$ °C, it is likely that the few crystalline particles present at low T_{treat} belong to the γ-Fe_2O_3 phase.

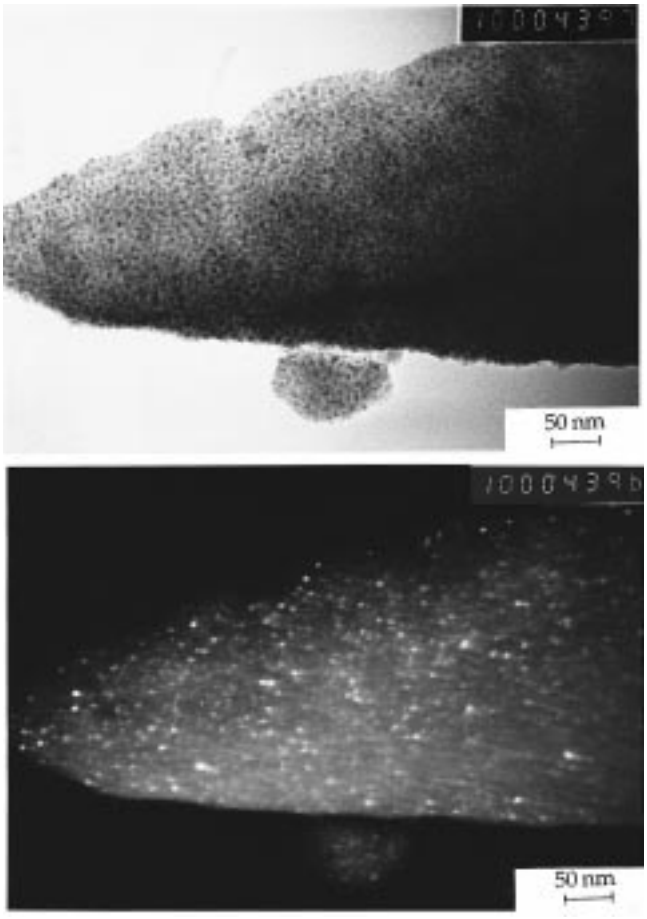

Figure 1. TEM (a, top) bright field and (b, bottom) dark field images of the $Fe_{28.5}900$ sample.

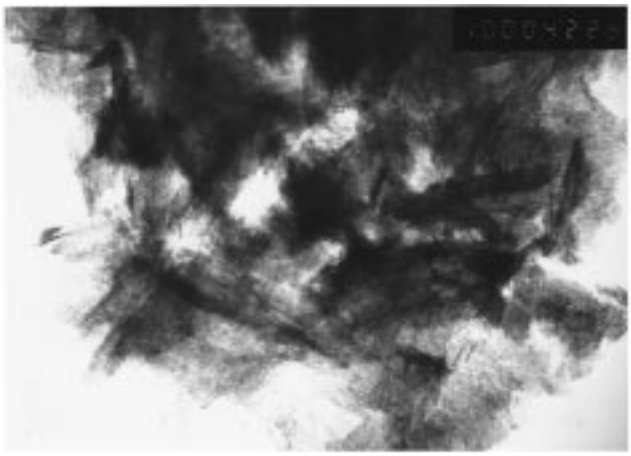

Figure 2. TEM bright field image of the $Fe_{33.2}300$ sample.

In Figure 4, the XRD spectra of the samples treated at 900 °C are reported. The structural modifications, observed in the previous work[15] on $Fe_{16.9}$ as a function of T_{treat}, become progressively more evident with increasing iron oxide content. Two peaks corresponding to the main reflections of the γ phase are present. Considering the ferrimagnetic behavior of the material and the thermal instability of the ferrimagnetic iron hydroxide at these T_{treat} values, the spectra unequivocally show the presence of an important amount of γ-Fe_2O_3. These two

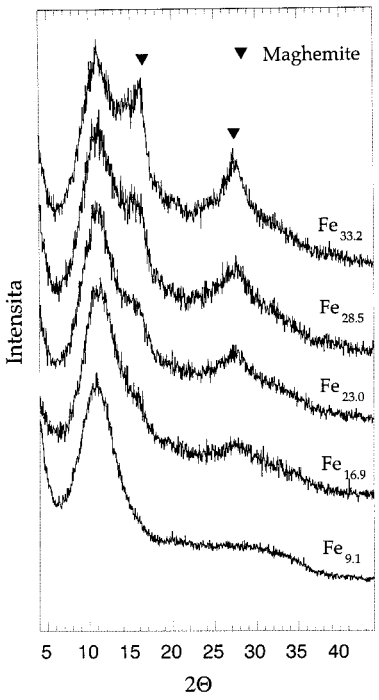

Figure 3. XRD data of all the Fe_x300 samples.

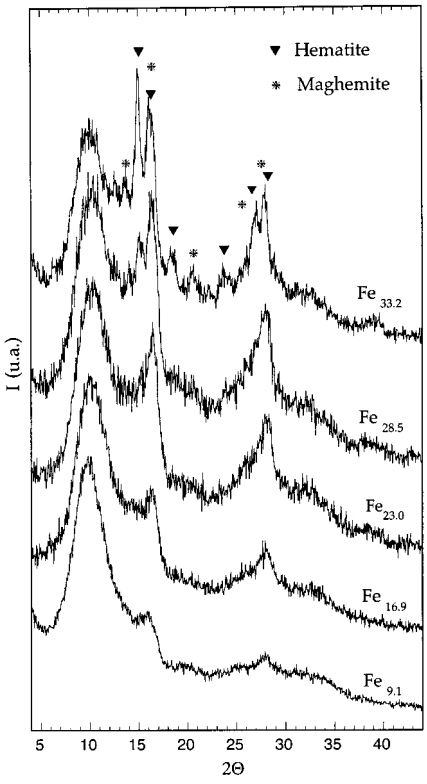

Figure 4. XRD data of all the Fe_x900 samples.

reflections are the only ones present in the spectra of $Fe_{9.1}$, $Fe_{16.9}$, and $Fe_{23.0}$, while in the $Fe_{28.5}$ and $Fe_{33.2}$ samples additional peaks appear. Since these are small peaks emerging on an amorphous background and since iron oxides are characterized by a series of very similar *d*-spacing values, their assignment is ambiguous. They could be attributable to the α-Fe_2O_3 antiferromagnetic phase, which is the most thermally stable form observed at high T_{treat}, but the alternative or simultaneous presence of the ϵ-Fe_2O_3 phase, also antiferromagnetic, cannot be excluded. This phase has already been observed in samples prepared with procedures[11] similar to that reported in the present paper, and its presence has been hypothesized in the study of $Fe_{16.9}$ samples.[15] The γ-to-α (and/or ϵ) transformation never goes to completion at the considered temperatures. In all the samples, the appearance of the new phases is accompanied by a further growth of the γ phase. It seems, therefore, that the progressive γ-to-α (and/or ϵ) transformation is accompanied by a contemporary growth of the γ phase at the expense of the residual amorphous phase. Structural modification of amorphous silica into crystobalite has been observed at higher temperatures for the samples with higher iron oxide contents and always at $T_{treat} > 1000$ °C. No iron(II) oxide phase has been evidenced, as also confirmed by Mössbauer spectroscopy.[22]

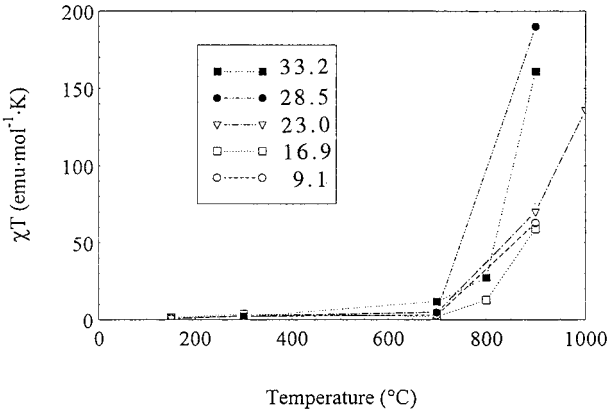

Figure 5. χT values measured at $T = T_{sep}$ as a function of T_{treat} for all the Fe_x samples.

Magnetic Measurements. The ZFC and FC magnetic susceptibilities were measured. In all the samples, the ZFC and FC susceptibilities coincide at high temperatures, while at lower temperatures they start to separate: the FC magnetization increases on decreasing the temperature, while the ZFC magnetization shows a broad maximum. Such behavior is characteristic of superparamagnetism,[23,24] i.e., of the temperature-dependent blocking of the magnetization of particles whose size determines a magnetic anisotropy comparable to thermal energy. Since the anisotropy is in a first approximation proportional to the volume of the particles, the blocking−deblocking process is different for particles of different size. The maximum temperature in the ZFC curve (T_{max}) is related in a complex way to the blocking of particles with average volume, while the temperature at which the ZFC and FC curves start to separate (T_{sep}) corresponds to the blocking of the largest particles. In all the measured samples, the FC curve never reaches saturation, thus indicating that, even at the lowest investigated temperature, a fraction of the particles is still in the superparamagnetic state.

For the samples treated at $T > 700$ °C, a dramatic increase in the χT value is observed on increasing T_{treat}. The χT values measured at $T = T_{sep}$ as a function of T_{treat} are reported in Figure 5. These results clearly indicate that between 700 and 900 °C, a broad transition occurs from an antiferromagnetic amorphous phase to a ferrimagnetic one, corresponding to γ-Fe_2O_3. For this reason, our attention has been devoted to the characterization of the magnetic properties of samples of the Fe_x900 series.

The temperature dependence of the ZFC and FC susceptibilities of these samples is shown in Figure 6. T_{max} increases from 3.5 K for the $Fe_{9.1}900$ sample up to 26 K for the $Fe_{33.2}900$ sample, while a larger increase is observed for T_{sep} (from 14 up to 116 K). The observed trend is due to an increase of the average volume and of the width of the distribution of the

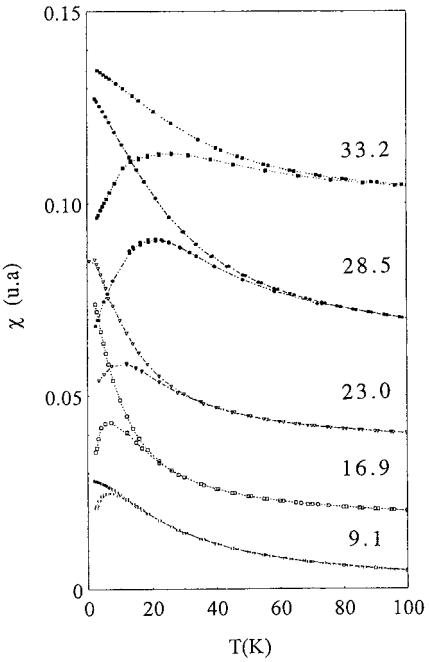

Figure 6. ZFC and FC magnetizations measured as a function of temperature for all the Fe_x900 samples. In all the pairs of curves, the upper one is FC and the lower is ZFC.

TABLE 1: Maximum Temperature (T_{max}) in the ZFC Curves and Temperature at Which the FC and ZFC Curves Start to Separate (T_{sep}) (Figure 5), Curie's Temperature (θ), Average Diameter (D_{av}), Standard Deviations of Distribution (σ), Residual Magnetization/Saturation Magnetization (M_r/M_S) and Coercivity (H_c)

sample Fe_x900	T_{max}, K	T_{sep}, K	θ, K	D_{av}, nm	σ	M_r/M_S	H_c, Oe
9.1	3.5	14	−0.48	2.7	0.27	0.13	80
16.9	5	26	1.48	2.8	0.43	0.22	570
23.0	12	35	0.30	3.1	0.47	0.22	650
28.5	21	73	6.24	3.6	0.65	0.29	1200
33.2	26	116	9.75	4.0	0.69	0.36	2000

particle size, as confirmed by TEM observations. However, also interparticle interactions that are expected to be higher in samples with higher iron concentrations can contribute to the observed shift.[14,25]

A rough evaluation of the strength of the interparticle interactions can be made by studying the dependence of χ on T. In fact, above T_{sep}, the susceptibility of an assembly of interacting superparamagnetic particles can be well reproduced by a Curie−Weiss law:

$$\chi = \mu^2(T)/[3k_B V(T - \theta)] \qquad (1)$$

where $\mu = M_S V$ is the magnetic moment of a particle, M_S being the saturation magnetization and V its volume, k_B is the Boltzmann constant, and θ is the so-called Curie temperature. However, because of the temperature dependence of M_S, $1/\chi$ is not linear in T. The temperature dependence of $M_S(T)$ follows the Bloch law, $M_S(T) = M_S(0)(1 - BT^{3/2})$.[23−25] The θ values, obtained by fitting the $1/\chi$ data with eq 1 and considering the thermal dependence of $M_S(T)$, are shown in Table 1. They seem to indicate that interparticle interactions are negligible for samples up to $Fe_{23.0}$, while they become relevant for samples with higher content.

Isothermal magnetization curves were measured up to 70 kOe at different temperatures. The results obtained at 70 K are shown in Figure 7. All the samples investigated are far from

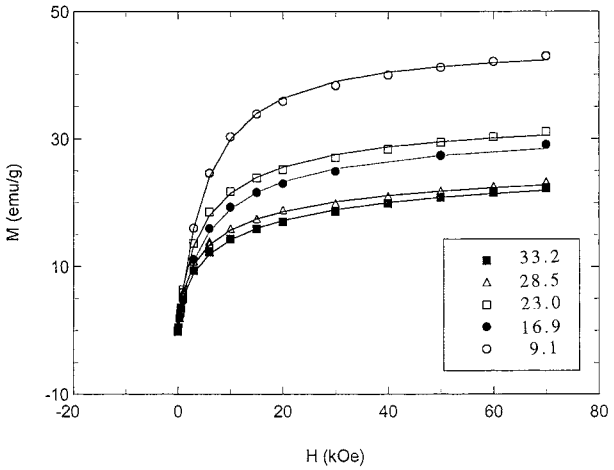

Figure 7. Experimental and calculated (solid line) magnetization curves for all the Fe_x900 samples.

being saturated, even at the lowest measuring temperature, and the saturation values extrapolated from the high field part of the curves measured at 3 K are much lower than that of the bulk γ-Fe_2O_3 (82 emu/g at 4.2 K).[13]

This behavior can in part be justified considering that the spins in nanometer sized magnetic particles are not fully aligned. This is a well-known phenomenon[3] that has been proved by different experimental tools.[26−28] Even if the real origin of spin canting is still controversial (it can be either a surface phenomenon or a finite size effect uniform throughout the particle[29]), it is, however, expected to increase with decreasing particle size. On the contrary, we observe lower M_S values in samples with higher iron content, which contain larger particles. The observed behavior can be explained by the presence of α-Fe_2O_3 (and/or ϵ-Fe_2O_3), whose contribution to M_S is much lower than that of γ-Fe_2O_3.

Information about the size distribution of the nanoparticles assemblies can be extracted from the magnetization curves, provided that the form of the distribution is known.[30] In fact, the magnetization of a system of identical, noninteracting, single-domain nanoparticles is described by the Langevin function:

$$L(\mu H/k_B T) = \coth(\mu H/k_B T) - k_B T/\mu H \qquad (2)$$

where $\mu = M_S V$ is the magnetic moment of a single particle and H is the external field. In a real system, the field dependence of M is given by the integral of the Langevin function over the size distribution. Then, assuming a certain form of size distribution and neglecting interparticle interactions, the mean particle diameter and the standard deviation (σ) can be evaluated. O'Grady and Bradbury[31] have suggested that a log-normal distribution can adequately describe the size distribution of a nanoparticle assembly, as later verified by several authors.[32−34]

The results of the fit are shown in Figure 7 together with the experimental curves. The average magnetic diameters have been evaluated by assuming a spherical shape of the particles and are reported in Table 1 together with the standard deviations of the distribution. The average diameter increases with the iron concentration, while the width of the distribution becomes progressively larger. The mean diameter values obtained in this way are smaller than those observed by electron transmission microscopy. This difference is due to the fact that the magnetic moment per particle is lower than the bulk value; i.e., it reflects the high ratio of surface to bulk. However, the observed increase of the width of the distribution seems to be reliable

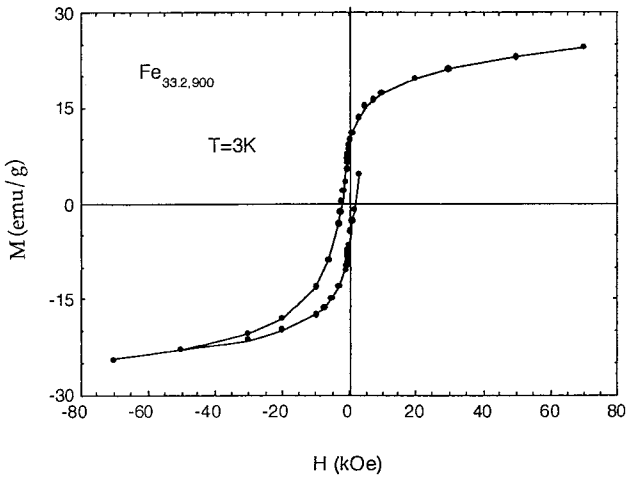

Figure 8. Magnetic hysteresis loop of the $Fe_{33.2}900$ samples measured at 3 K.

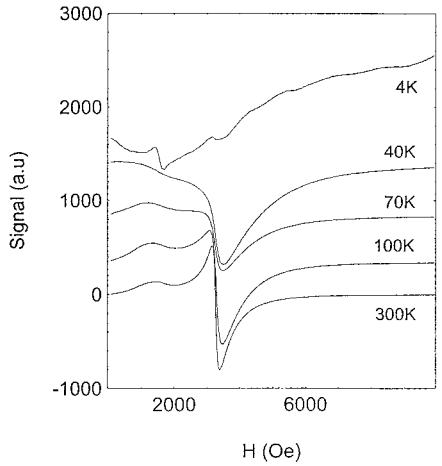

Figure 9. X-band EPR spectra of all the $Fe_{33.2}900$ sample between 4 and 300 K.

and is in good agreement with all the other experimental observations.

Hysteresis curves were collected in a field range of ±70 kOe, and that of $Fe_{33.2}900$ at 3 K is shown in Figure 8. The measured coercivities and the reduced remanences (M_r/M_S) are reported in Table 1. The $Fe_{9.2}900$ sample displays very low coercivity and remanence which can be due to the large fraction of fast relaxing particles present in this sample. Both the remanence and the coercivity increase strongly with the iron concentration, as expected for samples containing particles with progressively higher energy barriers. The coercivities become higher than that of bulk γ-Fe_2O_3, which ranges between 250 and 400 Oe. This is due to the single domain size of our samples: in this case, the hysteretic behavior originates from the fact that the time window of experimental investigation is shorter than the relaxation time of the magnetization.[24] The relaxation occurs through a coherent rotation of the spins which is energetically less favorable than the domain walls motion, responsible for the coercivity of the bulk materials.

We stress that, to our knowledge, the values of H_c observed in the $Fe_{33.2}900$ and $Fe_{28.5}900$ samples are among the highest values reported in the literature for maghemite nanoparticles of comparable size.[35,36] We believe that the iron oxide−matrix interface could strongly influence the coercivity of our nanocomposites. Since our samples contain very small particles, a large fraction of ions is at or near the surface so that the interaction between the iron oxide particles and the silica matrix may play a determinant role.

EPR. The EPR spectra of samples treated at temperatures up to 700 °C show two main signals located at $g \sim 2$ and g ∼ 4.3 which can be assigned to two different Fe(III) sites.[15,37] The $g \sim 2$ peak corresponds to a strongly interacting Fe^{3+} ion in an Fe_2O_3 particle, whereas the $g \sim 4.3$ peak corresponds either to a strongly distorted rhombic site located on the surface of the particle or to isolated iron(III) ions dispersed in the silica matrix. The position of the two lines is constant in the whole temperature range for all the samples, indicating the absence of internal fields and so of a blocked region. The ratio of the signal intensity at $g \sim 4.3$ to that at $g \sim 2$ decreases with increasing T_{treat} in all the samples.

The EPR spectra of samples treated at 900 °C display a highly symmetric peak located at $g \sim 2$ at room temperature. The $g \sim 4.3$ signal, even if weak, is still observed in all the spectra. On decreasing the temperature, the $g \sim 2$ peak becomes progressively broader with an asymmetric line shape. Such behavior is shown in Figure 9, where the temperature dependence of the EPR spectrum for the $Fe_{33.2}900$ sample in the 4−300 K range is reported.

According to Sharma and Waldner,[38] this peak can be assigned to the ferrimagnetic resonance of a random-oriented assembly of single-domain magnetic particles, while its temperature dependence can be explained by the Raikher and Stepanov model.[39] At low temperatures, the anisotropy energy barrier is larger than the thermal fluctuations and the absorption is smeared along the random distribution of the effective anisotropy fields H_a ($H_a = 2|K|/M$). On increasing the temperature, thermal fluctuations will lead to a decrease of the effective anisotropy field, whose temperature dependence is given by $H_a(T) = h_a(1/L(\xi) - 3/\xi)$, where h_a is the "true" anisotropic field, $\xi = MVH/k_BT$, and $L(\xi)$ is the Langevin function. Since we are dealing with real systems, where a distribution of both volumes and of easy axes occurs, the absorption will be distributed along the random direction of the anisotropy axes, thus providing an asymmetric line shape at low temperatures. Then the effect of temperature will be that of providing a progressively sharper and less asymmetrical line. At high temperatures, when the relaxation of the magnetization through the anisotropy energy barrier is much faster than the Larmor precession, thermal fluctuations will smear out the influence of the anisotropy: the resonance spectrum will be just like a normal paramagnetic resonance spectrum with a resonance at $h\nu = g\mu_B H$ and with a Lorentzian shape. Since line broadening is continuous with temperature, a characteristic blocking temperature cannot be defined.

A further contribution to the line width is given by interparticle interactions, which add a term to the local field. The line width of the absorption spectra at room temperature, when all the samples are fully superparamagnetic, slightly increases from 200 Oe for $Fe_{9.1}900$−$Fe_{23}900$ samples up to 250 Oe for higher iron concentrations. The observed trend suggests that interparticle interaction becomes relevant only for the $Fe_{28.5}900$ and $Fe_{33.2}900$ samples, a result that is in good agreement with the susceptibility measurements.

Discussion and Conclusions

Fe_2O_3−SiO_2 composites were prepared within a wide range of compositions. Superparamagnetic behavior is exhibited by all the samples, indicating that the size of the iron oxide grains is always in the nanometer range, even at the maximum iron content and/or after the highest thermal treatment (900 °C). The

increase of iron content gives rise to a small particle growth, while the spread of sizes around the average value increases in a more significant way. Similar effects are produced by the increase of treatment temperature of the samples. The small size increase is, however, sufficient to modify dramatically the hysteresis curves; consequently, the coercivity of the Fe_x900 samples strongly increases with concentration, reaching values among the highest reported in the literature for nanometer size maghemite. This indicates that the size range is between that of single-domain particles ($<15-20$ nm) and that of a superparamagnetic assembly of atoms (~ 1 nm).

Although the grain size grows slightly with heat treatments, the χT values measured at T_{sep} show a very steep increase after $T_{treat} > 700$ °C, indicating a massive formation of the ferrimagnetic γ-Fe_2O_3 phase at all the explored compositions. This result apparently contradicts the indications of XRD spectra, which show a gradual increase of the γ-Fe_2O_3 phase with the iron oxide content even in samples treated at 300 °C (Figure 1). Actually, this discrepancy is merely a consequence of the different features of the experimental data. In fact, a constant, even small percentage of γ-Fe_2O_3 in Fe_x300 samples increasingly influences the intensity of the peaks in the XRD spectra with increasing the iron oxide content, while susceptibility, which is expressed as emu per mole, is almost unaltered. Therefore, the experimental evidence is in favor of the maximum γ-Fe_2O_3 formation only after $T_{treat} > 700$ °C, while amorphous Fe_2O_3 is the most abundant phase in samples treated at $T_{treat} < 700$ °C, as confirmed by TEM dark field micrographs.

The result indicates that the stability of the iron oxide phases is strongly affected by the supporting material (host matrix), since γ-Fe_2O_3 is unstable in comparison with α-Fe_2O_3 at such high temperatures. The stabilizing effect of the support is further demonstrated by the poor sensitivity of the composites to prolonged thermal treatments; for instance, keeping the samples at a given temperature for 24 h does not modify the diffractometric or the magnetic response.

The variation of iron oxide content affects the abundance of γ-Fe_2O_3 formation, which reaches its maximum percent values in the more dilute samples ($Fe_{9.1}900$ and $Fe_{16.9}900$). In the more concentrated samples, α-Fe_2O_3 (and/or ϵ-Fe_2O_3) begins to form, while the amount of maghemite is still growing and is very abundant in $Fe_{33.2}900$. This result confirms the difficulty of obtaining only the γ phase, as discussed by authors who used a similar preparation method.[19,20] This phenomenon is probably caused by the growth of particle size in the iron-richer systems, since it has been observed that the increase of particle sizes favors the γ-to-α-Fe_2O_3 transition.[7] Another interpretation of the mechanism of maghemite formation has been given by del Monte et al.,[21] who suggest that the γ phase is formed through a reduction−oxidation reaction which is controlled by the amount of the organic species trapped inside the matrix pores. Certainly the presence of antiferromagnetic phases explains why the magnetization is higher in the dilute system rather than in the concentrated systems, contrary to the expectations coming from the growth of magnetic domains. The depression of magnetization in the concentrated samples can also in part be due to interparticle interactions, which have been evidenced by the fitting of $1/\chi$ versus T data. From this point of view, the method is satisfactory for the systems with low iron oxide content, while it needs improvement for the concentrated ones.

Acknowledgment. This work has been supported by CNR Grant 95.01588 CT 11 and MURST (Rome, Italy).

References and Notes

(1) Newnham, R. E.; McKinstry, S. E.; Ikawa, H. *Mater. Res. Soc. Symp. Proc.* **1990**, *175*, 161.
(2) Vollath, D.; Szabo , D. V.; Taylor, R. D.; Willis, J. O.; Sickafus, K. E. *Nanostruc. Mater.* **1995**, *6*, 941.
(3) Coey, J. M. D. *Phys Rev. Lett.* **1971**, *27*, 1140.
(4) Haneda, K.; Morrish, A. H. *Solid State Commun.* **1977**, *22*, 779.
(5) Morales, M. P.; Pecharroman, C.; Gonzales Carreño, T.; Serna, C. J. *J. Solid State Chem.* **1994**, *108*, 158.
(6) Kroll, E.; Winnik, F. M.; Ziolo, R. *Chem. Mater.* **1996**, *8*, 1594.
(7) Ayyub, P.; Multani, M.; Barma, M.; Polkar, V. R.; Vijayaraghavan, R. *J. Phys. C*: *Solid State Phys.* **1988**, *21*, 2229.
(8) Tronc E. *Nuovo Cimento* **1996**, *18D*, 163.
(9) Ida, T.; Tsuiki, H.; Ueno, A.; Tohji, K.; Udagawa, Y.; Iwai, K.; Sano, H.; *J. Catal.* **1987**, *106*, 428.
(10) Guglielmi, M.; Principi, G. *J. Non-Cryst. Solids* **1982**, *48*, 161.
(11) Chanéac, C.; Tronc E.; Jolivet, J. P. *Nanostruc. Mater.* **1995**, *6*, 715.
(12) Lund, C. R. F.; Dumesic, J. A. *J. Phys. Chem.* **1981**, *85*, 3175.
(13) Ziolo, R. F.; Giannelis, E. P.; Weinstein, B. A.; O'Horo, M. P.; Ganguly, B. N.; Mehrotra, V.; Russel M. W.; Huffman, D. R. *Science* **1992**, *257*, 219.
(14) Tronc, E.; Prene, P.; Jolivet, J. P.; d'Orazio, F.; Lucari, F.; Fiorani, D.; Godinho, M.; Cherkaoui, R.; Nogues, M.; Dormann, J. L. *Hyperfine Interact.* **1995**, *95*, 129.
(15) Concas, G.; Ennas, G.; Gatteschi, D.; Musinu, A.; Piccaluga, G.; Sangregorio, C.; Spano, G.; Stanger, J. L.; Zedda, D. *Chem. Mater.* **1998**, *10*, 495.
(16) Shull, R. D.; Ritter, J. J.; Shapiro, A. J.; Swartzendruber, L. J.; Bennet, L. H. *J. Appl. Phys.* **1990**, *67*, 4490.
(17) Roy, S.; Chatterjee, A.; Chakravorty, D. *J. Mater. Res.* **1993**, *8*, 689.
(18) Wang, J. P.; Luo, H. L. *J. Magn. Magn. Mater.* **1994**, *131*, 54.
(19) Ashua, M. N. *J. Mater. Sci. Lett.* **1993**, *12*, 1705.
(20) Niznansky, D.; Rehspringer, J. L.; Drillon, M. *IEEE Trans. Magn.* **1994**, *30*, 821.
(21) Del Monte, F.; Morales, M. P.; Levy, D.; Fernandez, A.; Ocaña, M.; Roig, A.; Molins, E.; O'Grady K.; Serna, C. J. *Langmuir* **1997**, *13*, 3627.
(22) Concas, G. Private communication.
(23) Morrish, A. H. *The Physical Principles of Magnetism*; John Wiley & Son: New York, 1965.
(24) Néel, L. *Ann. Geophys.* **1949**, *5*, 99.
(25) Djega-Mariadassou, C.; Dormann, J. L.; Nogués, M.; Villers, G.; Sayouri S. *IEEE Trans. Magn.* **1990**, *26*, 1819.
(26) Berkowitz, A. E.; Lahut, J. A.; Jacobs, I. S.; Levinson, L. M.; Forester, D. W.; *Phys. Rev. Lett.* **1975**, *34*, 594.
(27) Linderoth, S.; Hendriksen, P. V.; Bødker, F.; Wells, S.; Davies, K.; Charles, S. W.; Mørup, S. *J. Appl. Phys.* **1994**, *75*, 6583.
(28) Lin, D.; Nunes, A. A.; Majkrzak, C. F.; Berkowitz, A. E. *J. Magn. Magn. Mater.* **1995**, *145*, 343.
(29) Parker, F. T.; Foster, M. W.; Margulies, D. T.; Berkowitz, A. E. *Phys. Rev.* **1993**, *B47*, 7885.
(30) Chantrell, R. W.; Popplewell, J.; Charles, S. W. *IEEE Trans. Magn.* **1978**, *5*, 975.
(31) O'Grady, K.; Bradbury, A. *J. Magn. Magn. Mater.* **1994**, *39*, 91.
(32) Chien, C. L. In *Science and Technology of Nanostructured Magnetic Materials*; Hadjipanayis, G. G., Prinz, G. A., Eds.; NATO ASI Series B; Plenum: New York, 1991; p 477.
(33) Yaacob, I. I.; Nunes, A. C.; Bose, A. *J. Colloid Interface Sci.* **1995**, *171*, 73.
(34) Moumen, N.; Pileni, M. P. *Chem. Mater.* **1996**, *8*, 11128.
(35) Zhang, L.; Papaefthymiou, G. C.; Ying, J. Y. *J. Appl. Phys.* **1997**, *81* (10), 6892.
(36) Zhang, L.; Papaefthymiou, G. C.; Ziolo, R. F.; Ying, J. Y. *NanoStruct. Mater.* **1997**, *9*, 185.
(37) Tanaka, K.; Kamiya, K.; Matsuoka, M.; Yoko, T. *J. Non-Cryst. Solids* **1987**, *94*, 366.
(38) Sharma, V. K.; Waldner, F. *J. Appl. Phys.* **1977**, *48*, 4298.
(39) Raikher, Y. L.; Stepanov, V. I. *Phys. Rev. B* **1994**, *50*, 6250.